A Hybrid (Parabolic Equation)–(Gaussian Beam) Algorithm for Wave Propagation Through Large Inhomogeneous Regions

Bimba Rao and Lawrence Carin, *Senior Member, IEEE*

***Abstract*— The wide-angle split-step parabolic equation (PE) algorithm is used to model electromagnetic wave propagation over general inhomogeneous terrain up to a height h. The PE-computed fields at h are then projected onto a complete Gabor basis from which we effect Gaussian beam propagation at altitudes greater than h. The Gaussian beams can be propagated through general inhomogeneous media, devoid of failures at caustics and shadow boundaries (as befalls ray tracing). The accuracy of the Gaussian beam algorithm is demonstrated via two realistic examples: 1) low-frequency (HF) ionospheric propagation with application to over-the-horizon radar and 2) near-grazing high-frequency propagation for communication or surveillance applications. In the context of these examples, we discuss relevant numerical issues associated with the hybrid algorithm from which general advantages and disadvantages are addressed.**

***Index Terms*—Gaussian beams, nonhomogeneous media, propagation.**

I. Introduction

LONG-RANGE electromagnetic propagation is of interest for many applications, including radar [1] and communication [2] systems. For such problems, the propagation medium is often too complicated for Green's-function-based solutions or for the geometrical theory of diffraction [3]. Moreover, the propagation range is generally so large with respect to wavelength that rigorous numerical schemes such as the finite-difference time-domain [4], the method of moments [5], and the finite-element method [6] would require prohibitive computational resources. Therefore, there has recently been significant interest in the parabolic equation (PE) approximation to the Helmholtz wave equation, which yields a computationally efficient algorithm for long-range, forward-wave propagation through relatively general media [7]–[15]. Although the PE algorithm is approximate, upon comparison with rigorous schemes, it has been shown to yield highly accurate results [10], [11].

While the PE algorithm permits the accurate analysis of wave propagation over large ranges, finite computational resources ultimately limit the extent over which it can be applied. Therefore, researchers have sought the development of hybrid schemes that utilize the PE algorithm for complicated but relatively localized regions of the computational domain and alternative efficient schemes to extend the solution into the more "regular" regions. For example, Levy [13] used the standard "vertical PE" algorithm to model wave propagation over a rough ground or sea interface, while above a particular height, an efficient "horizontal PE" algorithm was applied. Additionally, Marcus [14] has matched the PE-computed fields to a Green's function appropriate for the region outside the PE algorithm's computational domain. In the work presented here we follow this strategy, but Gaussian beam propagation [17]–[21] is utilized to extend the fields beyond the region in which the PE algorithm is applied. This scheme is more flexible than the horizontal PE [13] or Green's function [14] algorithm in that it is applicable to general atmospheric inhomogeneities. Further, unlike ray-based codes [15], the beams are not subject to failure at shadow boundaries and caustics.

To effect the Gaussian beam strategy outlined above, one must self consistently extend the fields away from a given aperture field distribution. Here, we project the aperture fields rigorously onto a Gabor basis in a manner similar to that in [17]–[19]. One can show asymptotically that along the tilted axis of propagation (paraxially), the fields radiated by such Gabor basis functions constitute Gaussian beams [17]–[19]. The compact and analytic nature of such beam fields has motivated their application in a number of problems, including radome design [18]. However, nearly all previous research on Gaussian beam propagation away from an aperture has dealt with radiation in free-space (vacuum) [17]–[19] or has considered Gaussian beam interaction with *discrete* structures [18]. In these previous investigations, detailed studies have been undertaken on the asymptotic and numerical properties of Gabor-function-generated beams, yielding requirements for validity of common approximations (e.g., paraxial and far zone). In the work presented here, we are interested in Gaussian beam propagation away from an aperture into a general *inhomogeneous* medium. Therefore, we utilize the beams launched by the Gabor basis functions as *starter fields* for a Gaussian beam-tracing algorithm [20], [21] applicable to general continuously varying inhomogeneous media. The coupling of aperture theory with Gaussian beam tracing for inhomogeneous media places additional constraints on the Gabor-basis parameters, which have not been considered previously. In this paper, we discuss such issues in detail analytically, with demonstration provided by several numerical examples.

While Gaussian beam tracing through inhomogeneous media has been considered previously in acoustics [21] and seismology [20], such studies have treated the Gaussian beam

Manuscript received September 20, 1996; revised October 15, 1997.

The authors are with the Department of Electrical and Computer Engineering, Duke University, Durham, NC 27708 USA.

Publisher Item Identifier S 0018-926X(98)03403-6.

excitation in an admittedly *ad hoc* manner [20], [21]. In the work presented here, we place the launching of such Gaussian beams on a firm mathematical footing, through use of the well-known Gabor expansion. Therefore, the principal contribution of this paper is the coupling of the Gabor transform with Gaussian beam propagation for inhomogeneous media. While the Gabor expansion and beam tracing are well known individually, their coupling is believed to be new. Moreover, as alluded to above, this synergy introduces new constraints on the Gabor expansion functions, which are shown to be dictated by the detailed characteristics of the inhomogeneous medium through which the beams are traced. The resulting (Gabor expansion)–(Gaussian beam tracing) algorithm provides a new method of extending the PE-generated fields beyond a predefined aperture, into an inhomogeneous medium. This hybrid scheme is applicable to general inhomogeneities, thereby avoiding previous restrictions to particular inhomogeneity profiles [13] or specialized Green's function [14]. However, the details of the Gabor expansion introduce advantages and disadvantages to the use of this method for extending the PE-generated fields, with such issues addressed in detail through consideration of examples.

The remainder of the paper is organized as follows. In Section II, we give a brief summary of the wide-angle PE algorithm, followed by a detailed explanation of how the PE fields are extended by Gaussian beam tracing. The new constraints on the Gabor aperture expansion are discussed and demonstrated numerically in subsequent examples. The accuracy of the beam-tracing algorithm is calibrated in Section III, through consideration of two realistic examples of interest to radar and communication applications. Finally, conclusions are summarized in Section IV.

II. Formulation

A. Parabolic Equation

The parabolic equation (PE) method has been utilized for over half a century [7]–[15] to model long-range wave propagation through the atmosphere. Here, we describe how the PE method can be coupled rigorously with Gaussian beam algorithms to model propagation through general inhomogeneous regions. Such that the discussion is self contained, we briefly review key aspects of the PE method, before proceeding to the hybrid PE-(Gaussian beam) formulation.

For vertical and horizontal polarization, respectively, we define $u_v(\boldsymbol{r})$ and $u_h(\boldsymbol{r})$ [12] as

$$u_v(\boldsymbol{r}) = \sqrt{\frac{r\sin\theta}{\epsilon_r}}\, H_\phi(\boldsymbol{r}), \quad u_h(\boldsymbol{r}) = \sqrt{r\sin\theta}\, E_\phi(\boldsymbol{r}) \tag{1}$$

with $\epsilon(\boldsymbol{r})$ representing the inhomogeneous medium permittivity, an $\exp(j\omega t)$ time dependence is suppressed, and the spherical coordinate system has its origin at the earth center. Defining the $r\theta$ plane as containing the transmitting and receiving antennas, we utilize the "earth flattening" relations [12], [22], [23] $x = a\theta$ and $z = a\ln(r/a)$, where a is the earth radius. The wave equation in the xz coordinate system is then

$$\frac{\partial^2 u}{\partial z^2} + \frac{\partial^2 u}{\partial x^2} + K^2(x,z)u = 0 \tag{2}$$

where

$$K_h(x,z)^2 \approx k_o^2\epsilon(\boldsymbol{r})(r/a)^2 - \frac{3}{4x^2}$$
$$K_v^2(x,z) \approx k_o^2\epsilon(\boldsymbol{r})(1+2z/a)^2 - \frac{3}{4x^2} \tag{3}$$

with $k_o = \omega(\mu_o\epsilon_o)^{1/2}$; the approximations in (3) are valid for $x \ll a$ and $z \ll a$. As will be discussed below, the singularity in (3) due to the source at $x = 0$ does not cause a problem when implementing the PE approximation to (2).

Using operator notation, we write (2) as

$$(\partial/\partial x + jQ)(\partial/\partial x - jQ)u(x,z) + j[\partial/\partial x, Q]u(x,z) = 0$$
$$Q(x,z) = \sqrt{\partial^2/\partial z^2 + K^2(x,z)} \tag{4}$$

where $[\partial/\partial x, Q] = \partial/\partial x Q - Q\partial/\partial x$ is the commutator of the operators $\partial/\partial x$ and Q. For range-independent media $(\partial/\partial x K = 0)$, the commutator vanishes and we obtain the exact one-way parabolic equation

$$\partial u(x,z)/\partial x = -jQ(z)u(x,z) \tag{5}$$

which has the formal solution

$$u(\Delta x, z) = \exp[-j\Delta Q]u(0,z) \tag{6}$$

We solve (6) approximately via the well-known wide-angle, split-step algorithm [9], [10]; in this scheme, the down-range discretization (x) is generally large compared to wavelength λ, so $k_o^2 \gg 1/x^2$ at the sample points and, therefore, we can ignore the $-3/4x^2$ terms in (3). It should be pointed out that (5) is exact for range-independent media (prior to approximating Q), but it can be used approximately for propagation in range-dependent $(\partial/\partial x K \neq 0)$ environments [7]–[15].

B. Gabor Transform

While the wide-angle PE algorithm can, in principle, be applied to compute the fields up to arbitrary altitudes (z), in practice, the height to which such computations can be performed is limited by the computational resources available. For ionospheric propagation, for example, it is difficult to model the entire computational domain (from the earth surface to the upper ionosphere) via the PE algorithm. This suggests a hybrid scheme in which the PE algorithm is utilized to model electromagnetic propagation near the earth surface, up to a height $z = h$, taking proper account of surface roughness and an imperfectly conducting earth [11]–[13]; the PE-computed fields at $z = h$ are then used by a separate efficient algorithm to handle propagation for $z > h$. This strategy has been pursued by several authors [13]–[15], but all such previous schemes have invoked various simplifying assumptions (e.g., that the atmosphere has a "standard" profile [13], that a Green's function can be found for the outer region [14] and that simple ray tracing is applicable [15]). In many applications, however, such assumptions are inappropriate and, therefore, here we demonstrate how the fields at $z > h$ can be computed rigorously via Gaussian beam propagation. Gaussian beams represent a natural extension of ray codes [24] and are

applicable to general atmospheric profiles; unlike ray codes, the beam-tracing algorithm does not have problems at caustics and shadow boundaries.

Let the PE-computed fields at $z = h$ be represented by $f(x)$, where $f(x)$ is E_ϕ for horizontal polarization and H_ϕ for vertical polarization. If we assume that the region $z > h$ is characterized by a *homogeneous* medium with wavenumber k, then $\boldsymbol{E}(x, z > h) = -\nabla \times \psi y$ for horizontal polarization and $\boldsymbol{H}(x, z) = \nabla \times \psi y$ for vertical polarization ($y = -x \times z$), where

$$\psi(x, z) = 2 \int_{-\infty}^{\infty} f(x') G_f(x, z; x', 0)\, dx' \tag{7}$$

and

$$G_f(x, z; x', z') = -\frac{j}{4} H_o^{(2)}(kR)$$
$$R = \sqrt{(x - x')^2 + (z - z')^2} \tag{8}$$

In theory, the integral in (7) is taken over the entire surface at $z = h$ (such that the equivalence and image theorems from which (7) is derived are valid); however, in practice, we integrate over the region x' that contributes significantly to the fields of interest in $z > h$. It is interesting to note that, through the earth-flattening transformation used in the PE algorithm discussed in Section II-A, the PE-computed fields at $z = h, f(x)$ fit naturally within the Cartesian coordinate system employed here and below, despite the curved nature of the earth.

Following [17]–[19], we expand the fields $f(x)$ in Gaussian beams by employing the Gabor transform

$$f(x) = (\sqrt{2}/L_x)^{1/2} \sum_m \sum_n a_{mn} \exp[-\pi(x - mL_x)^2/L_x^2] \cdot \exp(jnk_x x), \qquad L_x k_x = 2\pi \tag{9}$$

The coefficients a_{mn} can be determined via a well-known biorthogonality condition [17]–[19]. While the summations in (9) are theoretically of infinite extent, as is customary, we only include those modes that are propagating [17]–[19]. Defining $\psi_{mn}(x, z)$ as the fields produced by the mnth modulated Gaussian, we have

$$\psi_{mn}(x, z) = 2(\sqrt{2}/L_x)^{1/2} \int_{-\infty}^{\infty} G_f(x, z; x', 0) \cdot \exp[-\pi(x' - mL_x)^2/L_x^2] \exp(jnk_x x')\, dx'. \tag{10}$$

From standard asymptotics, one can show that [25]

$$\psi_{mn}(x, z) \sim \exp(-j\pi/4) \frac{2^{1/4}}{\pi} \sqrt{\frac{L_x \lambda}{z_R + jb}} \cdot \exp\left[-jk\left(z_R + \frac{1}{2} \frac{x_R^2}{z_R + jb)}\right)\right]$$
$$b = L_x^2 \cos^2 \theta_x / \lambda \tag{11}$$

where $\lambda = 2\pi/k$, $\theta_n = \sin^{-1}(nk_x/k)$, and (x_R, z_R) corresponds to a coordinate system rotated to the angle θ_n (see Fig. 1). The result in (11) is valid in the paraxial limit $x_R \leq |z_R + j_b|$ and corresponds to a wave traveling in the $+z_R$ direction with a Gaussian amplitude profile; the beam radius at which the amplitude decreases to $1/e$ of its value on axis is

$$B(z_R, L_x) \equiv \sqrt{\frac{2}{k} \frac{z_R^2 + b^2}{b}}. \tag{12}$$

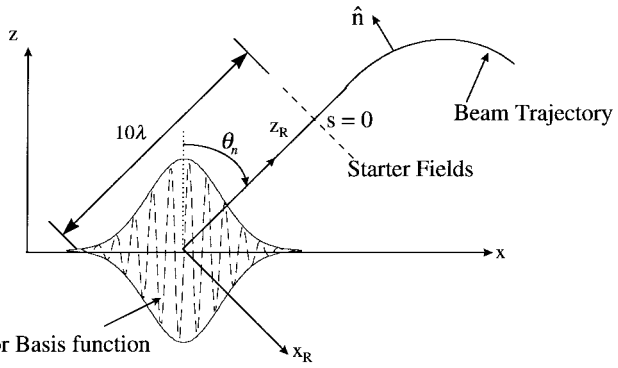

Fig. 1. Rotated coordinate system used to define the asymptotic behavior of the fields radiated from a Gabor basis function with spectral wavenumber nk_x and propagation angle $\theta_n = \sin^{-1}(nk_x/k)$ for wavenumber k [see (11)]. The asymptotic fields are used at $z_R = 10\lambda$ as starter fields for the general Gaussian beam scheme detailed in (15)–(19) and the unit vector $\hat{\boldsymbol{n}}$ is normal to the ray trajectory.

Before proceeding, we consider several properties associated with the approximation in (11). In particular, note that the Gabor size L_x required to achieve a given b is

$$L_x \geq \sqrt{b\lambda}/\cos\theta_n \tag{13}$$

for all θ_n of importance. Therefore, for angles near grazing ($\theta_n \approx \pi/2$), which may be of interest for some PE applications, the basis size L_x required for a desired beamwidth [see (12)] may be quite large. Additionally, it has been shown that the asymptotic result in (11) is valid for observation points

$$z_{Rn} \gg b_n = (L_x \cos\theta_n)^2/\lambda. \tag{14}$$

For the numerical examples considered here, we have found the asymptotic results to be accurate for $z_R \geq 10\lambda$. Therefore, (13) is the principal constraint of interest here; it and a new requirement, introduced by Gaussian beam propagation through inhomogeneous media, will be studied in detail in the subsequent numerical examples.

The Gaussian beam fields in (11) for appropriate Gabor width L_x serve as starter fields for a subsequent beam-tracing algorithm applicable to inhomogeneous media. We typically start the beam-tracing algorithm at $z_R = 10\lambda$ at which point, as mentioned, the asymptotic beam profile in (11) has been found to be accurate. Recall that (11) was derived assuming that the region $z > h$ is characterized by *homogeneous* wavenumber k. Thus, for it to be a valid starter field, we require the region $h \leq z \leq h + 10\lambda$ to be homogeneous with wavenumber k. From (3), we see that the earth-flattening transformation results in a z-dependent atmosphere, even in regions where the original dielectric constant $\epsilon(\boldsymbol{r})$ is homogeneous. However, for most frequencies of interest, 10λ is sufficiently small compared to the earth radius a, which, practically speaking, the homogeneity condition required of (11) is met easily.

C. Beam Tracing

As discussed with respect to (10) and (11), several authors [17]–[19] have developed beam codes for propagation away from apertures; however, these formulations assume that the medium is described by the homogeneous wavenumber k and are not easily extended to general inhomogeneous media (although they have been applied successfully for propagation through canonical inhomogeneous environments [17]–[19]). Therefore, we utilize the Gaussian beams in (11) as starter fields for a beam-tracing algorithm that is applicable for wave propagation through *general* inhomogeneous media. In particular, we have adapted the beam-tracing algorithm first developed by Červený *et al*. [20] in the geophysical literature and later applied by Porter and Bucker [21] in underwater acoustics. A succinct summary of this algorithm is given here.

Solutions are sought for the homogeneous wave equation

$$\frac{\partial^2 u(x,z)}{\partial x^2} + \frac{\partial^2 u(x,z)}{\partial z^2} + \frac{\omega^2}{c^2(\boldsymbol{r})}\, u(x,z) = 0 \qquad (15)$$

where $c(\boldsymbol{r})$ is the inhomogeneous wave velocity. The equation is solved under the *parabolic* approximation, with forward-wave propagation along the ray paths characteristic of conventional ray tracing [26]. Interestingly, our final scheme is, therefore, a hybrid solution of two different parabolic equations: one describing general forward-wave propagation in an earth-flattened environment and the other representing forward-wave propagation along conventional ray trajectories. The ray trajectories, defined by the vector $\boldsymbol{t}$, satisfy [26]

$$\frac{d}{ds}\left(\frac{1}{c}\,\frac{d\boldsymbol{t}}{ds}\right) = -\frac{1}{c^2}\,\nabla c \qquad (16)$$

where s is the distance along the ray trajectory ($|d\boldsymbol{t}/ds| = 1$). Along the trajectories (16), the parabolic approximation to (15) satisfies [20], [21]

$$u(s,n) = U(s,n)\exp\left(-j\omega \int_{s_o}^{s} \frac{ds}{c(s)}\right) \qquad (17)$$

where s_o represents the start point along the ray trajectory and n is normal to the ray path (Fig. 1). In classical ray tracing, the n dependence of $U(s,n)$ is neglected, while here, in the context of Gaussian beam tracing, we consider

$$U(s,n) = A\sqrt{c(s)/q(s)}\exp\left(\frac{-j\omega}{2}\,\frac{p}{q}\,n^2\right). \qquad (18)$$

For (17) and (18) to constitute a solution to the parabolic wave equation, we find that [20], [21]

$$\partial q/\partial s = cp \quad \partial p/\partial s = -\frac{c_{nn}}{c^2}\,q \qquad (19)$$

where $c_{nn} = \partial^2 c/\partial n^2$ evaluated at $n = 0$.

To use this beam solution in the context of a hybrid PE-(Gaussian beam) algorithm, at the launch point of the Gaussian beam [see Fig. 1], we match (18) to (11) by setting $q(s=0) = c(s=0)/(z_R + jb)$ and $p(s=0) = 1$; the constant A in (18) can be determined easily by matching (17) and (18) to the remaining terms in (11). The beam is then traced away from the launch point $s = 0$ as in conventional ray tracing, with $q(s)$ and $p(s)$ updated continuously by employing a finite-difference approximation to (19) [21]. In conventional ray tracing $q(s)$ is real and caustics occur at $q(s) = 0$; in beam tracing, $q(s)$ is complex and caustics are, therefore, avoided.

It is important to address the inherent approximations in the beam-tracing scheme such that algorithm parameters are selected appropriately. From (19), the beam characteristics are dictated entirely by the c and c_{nn} in the vicinity of the ray trajectory $\boldsymbol{t}$. Therefore, implicitly, it is assumed that the Gaussian beamwidth B is tight enough such that the material properties do not vary too quickly as one moves away from the ray path (beam axis). This, therefore, introduces a new requirement on the Gabor parameters, which has not been examined to date. The beamwidth at a given angle θ_n is dictated from (11) and (12) by the Gabor width L_x. Therefore, L_x must be selected appropriately as to assure the accuracy of (17)–(19), introducing a new constraint in addition to the well-known (13) and (14).

The issue of how tight the Gaussian beams must be relative to the material inhomogeneities has not been studied in detail to date. To address this issue, we introduce the parameter

$$\gamma(\boldsymbol{r}, L_z) \equiv \frac{\dfrac{\dot{\partial}}{\partial n}\sqrt{\epsilon(\boldsymbol{r})}}{\sqrt{\epsilon(\boldsymbol{r})}}\, B(\boldsymbol{r}, L_x) \qquad (20)$$

which quantifies the relative change in the index of refraction over the beamwidth $B(\boldsymbol{r})$, where $\boldsymbol{r}$ exists along the beam axis. It is of interest to determine how small γ must be to assure accurate beam-tracing results. This places constraints on the Gabor-basis width L_x, with the ultimate limit on γ dictated by the wavelength of operation. A detailed consideration of such issues is addressed below when addressing the numerical examples.

III. Examples

A. Over-the-Horizon Radar

We consider the numerical properties of the hybrid scheme introduced above by first considering an example of interest to over-the-horizon radar (OTHR). In OTHR applications, one must track electromagnetic propagation over thousands of kilometers, through highly inhomogeneous media [16], usually in the HF frequency band. An example refractive-index profile [16] is shown in Fig. 2 as a function of height for a frequency of 10 MHz. The beam tracing code of Sections II-B and C does not require the index of refraction to be independent of the spherical coordinate ϕ, although we make that assumption here (this assumption is often also made in actual OTHR systems [16], [27]). We compute the fields via PE up to a height of 2 km in the earth-flattened environment and store the fields at height $h = 1$ km as a function of transverse distance x, up to a distance $x = 5$ km at which the radiated fields are negligible. For simplicity, we consider the earth to be smooth with soil characterized by the complex permittivity 2-j.01; one could use far more complicated (and, perhaps, realistic) earth profiles in the PE algorithm [7]–[15], but our motivation here is to demonstrate the hybrid PE-beam scheme, not to present

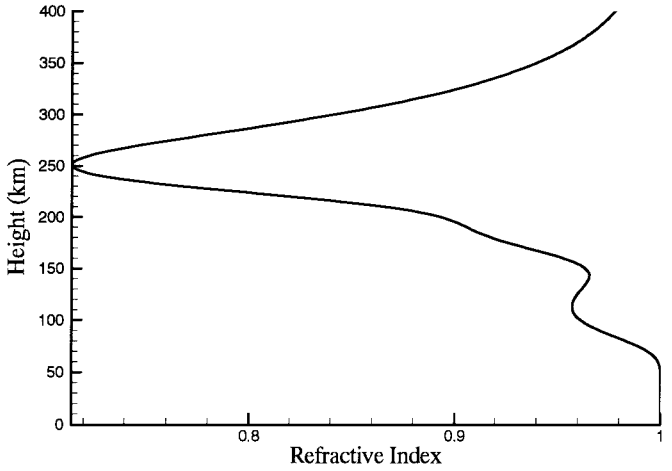

Fig. 2. Refractive-index profile used in the ionospheric wave-propagation example.

the most sophisticated application of the PE approximation, which has been done elsewhere [7]–[15].

In the PE algorithm, we require a starter field at $x = 0$ as a function of height z. There are many options available, but we have picked the distribution [12] (for the horizontally polarized example considered here)

$$E_\phi(x = 0, z) = \exp[-(z - z_o)^2/2\sigma^2] \cdot \exp(-jk \sin\theta_o z) \tag{21}$$

where $z_o = 200$ m, $\sigma = 75$ m, $\theta_o = 28.6°$, $k = 2\pi/\lambda$, and $\lambda = 30$ m. The wide-angle PE-computed fields are presented in Fig. 3, with the dashed line identifying the aperture over which the fields are stored for subsequent beam propagation. The magnitude of these aperture fields are plotted in Fig. 4 where we see a peak field near 2 km, which is consistent with predominant field propagation at the angle $\theta = 28.6°$, as prescribed by (21). These aperture fields $f(x)$ are then subjected to the Gabor transform in (9).

The first numerical issue we address is the coupling of the PE solution with the Gabor expansion reviewed in Section II-B. In the PE computations, the fields are discretized coarsely (relative to wavelength) in the longitudinal direction, the highly oscillatory $\exp(-jkx)$ term having been extracted prior to the PE analysis [7]–[13]. However, the Gabor expansion requires subwavelength discretization to assure algorithm accuracy. This issue is easily handled by interpolating the slowly varying term computed via the PE (we have utilized spline interpolation here). Therefore, the coupling of these two algorithms presents little difficulty in this connection.

With regard to the parameter L_x used in the Gabor expansion, care must be taken to assure that the beams are sufficiently tight such that the ionospheric inhomogeneities are sampled properly in the beam-tracing algorithm of Section II-C. This issue was addressed through introduction of the parameter $\gamma(r, L_x)$ in (20). Several of the ray trajectories are plotted in Fig. 5, for the profile in Fig. 2, and the complicated refractive-index profile results in interesting ray trajectories, only a few of which are shown here for clarity. To determine the effects of the beamwidth on the accuracy of the beam-

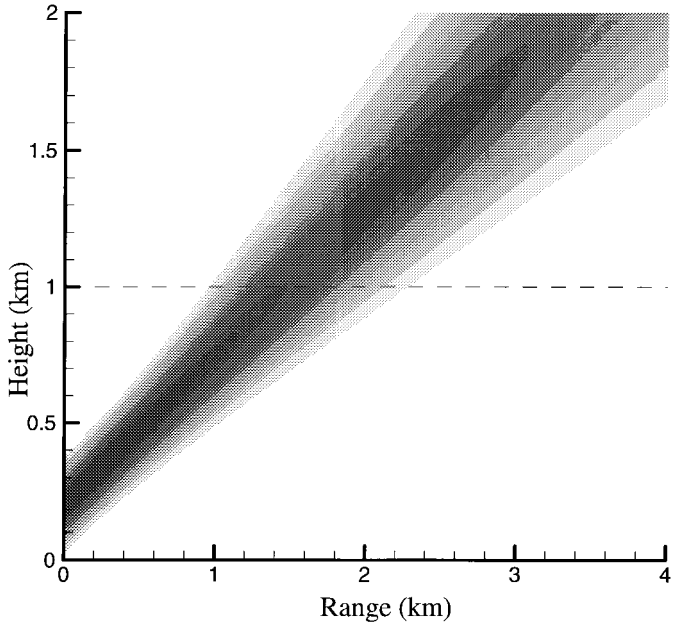

Fig. 3. Magnitude of the fields computed via a split-step wide-angle parabolic equation analysis for radiation above the earth. Results are plotted in the "earth-flattened" coordinate system and the initial field profile is described in (21).

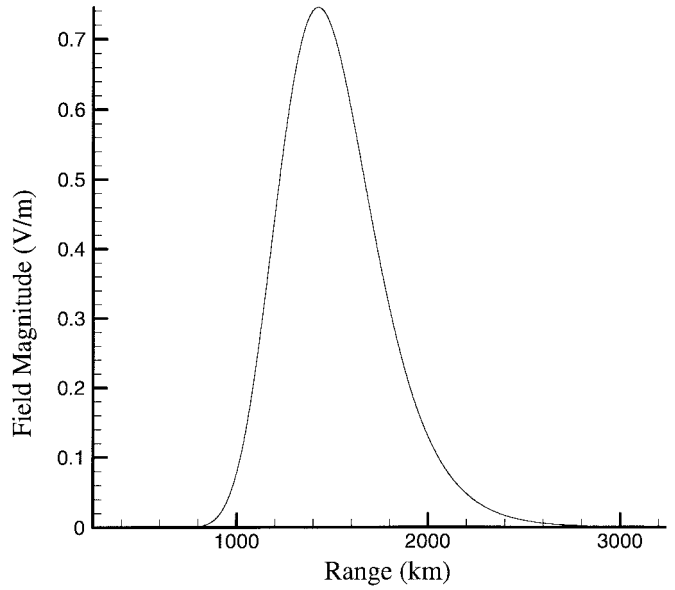

Fig. 4. Magnitude of the electric fields computed in Fig. 3, observed on the dashed curve denoted there.

tracing results, we consider a representative beam from Fig. 5, highlighted there in bold (corresponding to a launch angle of 28.6° from (21) characteristic of the principal propagation direction). In Fig. 6, we plot the beamwidth, as measured at the receiver with the initial beamwidth (at the launch) as a parameter; since the initial beamwidth is a function of L_x, variation of the beamwidth B in Fig. 6 is equivalent to varying L_x. As expected, for small B the final beamwidth is quite large. A minimum beamwidth is achieved near $L_x = 12$ km, followed by an approximately linear increase with increasing L_x. As mentioned above, the Gabor-generated Gaussian beams are matched to the beam-tracing algorithm 10λ from the

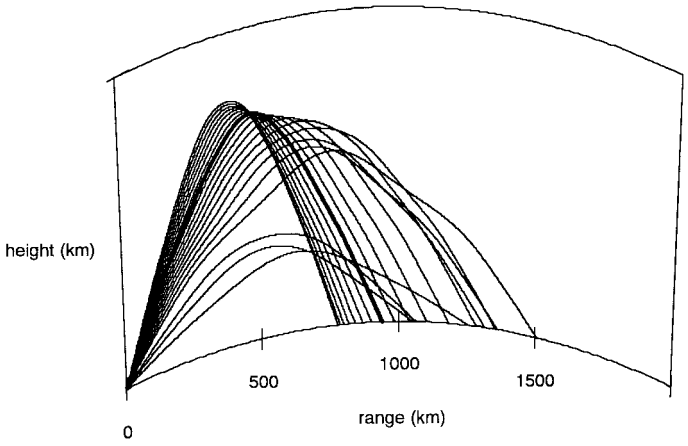

Fig. 5. Example beam trajectories for the Gabor-excited beams representative of the fields in Fig. 4 for the refractive-index profile described in Fig. 2. The bold curve corresponds to a launch angle of 28.6°.

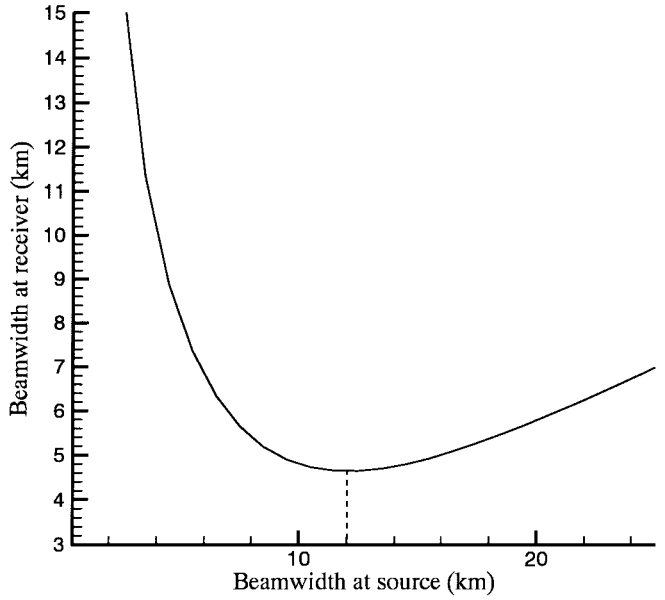

Fig. 6. Beamwidth of the bold beam in Fig. 5, as a function of the beamwidth at the launch of the Gaussian beam (or, equivalently, as a function of the Gabor parameter L_x). The minimum occurs for $L_x = 12$ km.

aperture, at which the asymptotic expression in (11) was found accurate for all L_x considered. Therefore, the accuracy of the subsequent results, as a function of L_x, are dictated by the degree to which the approximations in the beam-tracing scheme are accurate, i.e., whether the consequent beamwidths are sufficiently small for the inhomogeneity considered here.

In Fig. 7 is plotted the parameter $\gamma(\boldsymbol{r}, L_x)$ for the representative beam considered above, as a function of height for $L_x = 12$ km (which, from Fig. 6, gives the tightest beam). The dashed lines indicate the maximum height achieved by this beam; at this height the beam cross section is parallel to the direction of the inhomogeneity and, therefore, $\gamma(\boldsymbol{r}, L_x)$ is maximum at this point. We see that the maximum change in the index of refraction over the beamwidth is less than 2%. Since the maximum variation occurs at the peak height of the beam, in Fig. 8 we plot $\gamma(\boldsymbol{r}, L_x)$ at this point, as a function of the Gabor parameter L_x. The left-most vertical dashed line represents the value of L_x required such that the

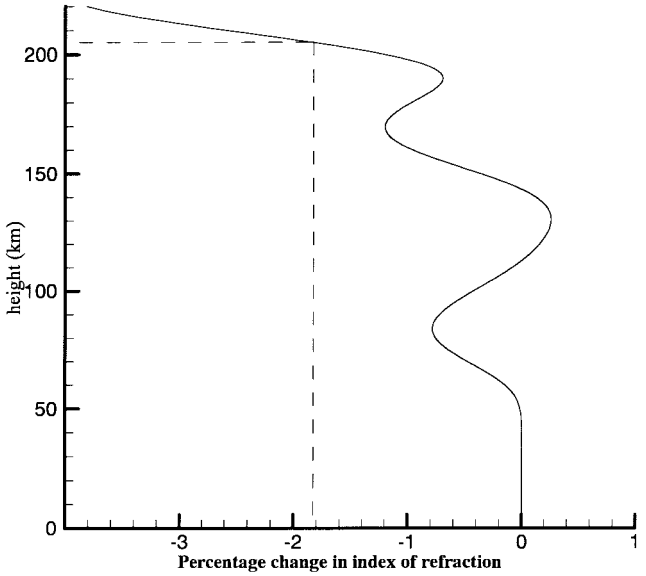

Fig. 7. The height-dependent change in the refractive index over the beamwidth for the bold beam in Fig. 5. The refractive-index change is defined by $\gamma(\boldsymbol{r}, L_x)$ from (20). We consider the index-of-refraction profile in Fig. 2 and use $L_x = 12$ km, which corresponds to the minimum in Fig. 6.

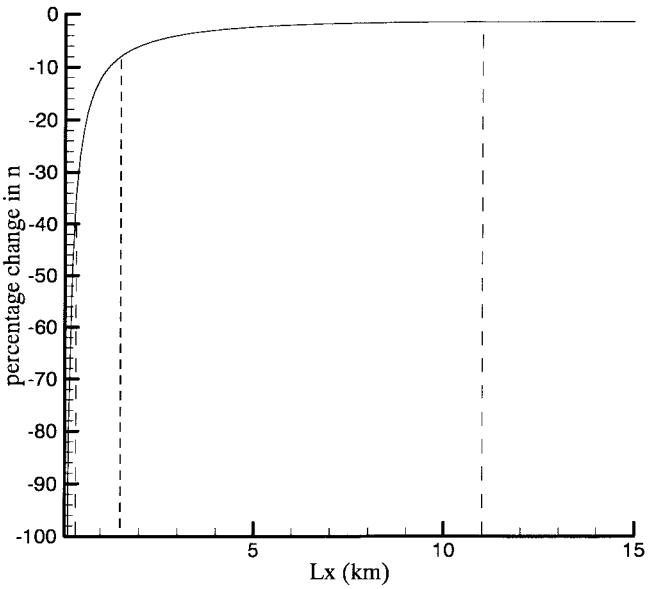

Fig. 8. Change in the refractive index over the beamwidth for the bold beam in Fig. 5. The refractive-index change is defined by $\gamma(\boldsymbol{r}, L_x)$ in (20), as measured at the inflection point (peak height) of this beam [see Fig. 5]. The parameter $\gamma(\boldsymbol{r}, L_x)$ is plotted as a function of the Gabor-expansion width L_x.

paraxial approximation is valid 10λ from the aperture at which the Gabor fields are matched to the beam-tracing algorithm. While satisfaction of the paraxial and far-zone approximations are sufficient for free-space applications, here we have the additional constraint that the beam must be tight enough such that the underlying assumptions in the beam-tracing algorithm are appropriate. We see from Fig. 8 that the value of L_x required of the paraxial approximation results in a 40% change in the index of refraction over the beamwidth $(\gamma(\boldsymbol{r}, L_x) = 0.4)$ at the point of inflection (peak beam height). The beam-tracing results for this value of L_x were meaningless and are not presented. However, in Fig. 9 are plotted the results of the

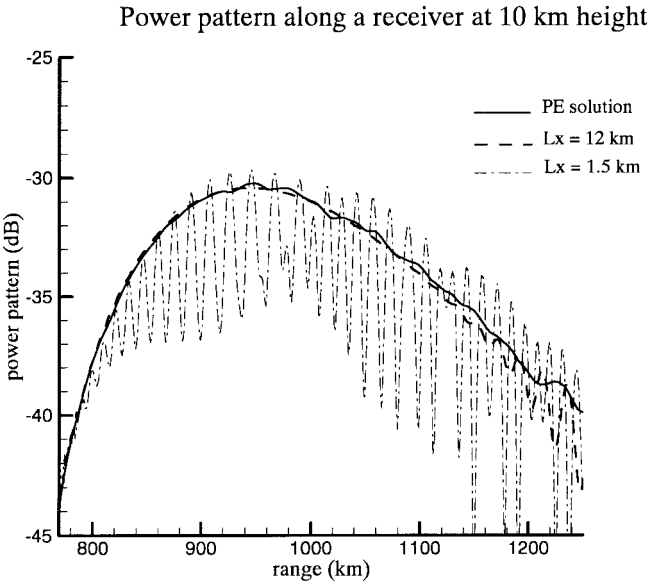

Fig. 9. Comparison of the fields radiated through the profile in Fig. 2 for the initial field distribution in (21). The dashed curves correspond to solutions from the hybrid PE (Gabor expansion–beam tracing) algorithm while the solid curve corresponds to the solution from the full PE algorithm (over the entire computational domain). With regard to the former, results are shown using Gabor widths of $L_x = 1.5$ km and $L_x = 12$ km and all results are plotted for an observation height of 10 km.

Gaussian beam tracing for $L_x = 1.5$ km and $L_x = 12$ km, as observed as a function of range at an altitude of 10 km. We see from these results that $L_x = 1.5$ km, which corresponds to a maximum change in the index of refraction of 8% over the beamwidth (Fig. 8), yields results that are inaccurate relative to the full-PE solution (in which the PE algorithm was used to calculate fields over the entire domain, with results shown in Fig. 10). The beam-tracing results in Fig. 9 for $L_x = 12$ km (which corresponds from Fig. 5 to the tightest beamwidth) yield good agreement compared to the full PE results.

Before proceeding, we summarize the conclusions of this numerical study for OTHR. We have found that the well-known constraint on L_x, dictated by the paraxial approximation, may be inadequate for applications involving inhomogeneous medium. In particular, the beamwidth must be narrow enough over the range of propagation, relative to the material inhomogeneity, such that the underlying assumptions required of beam-tracing are met. In particular, we require that the dynamics of beam propagation are dictated primarily by the electrical properties near the beam axis. For this to hold, material properties must change slowly over the beamwidth. This led us to develop a new parameter $\gamma(\boldsymbol{r}, L_x)$, which quantifies the relative change in the index of refraction over the r-dependent beamwidth. For the numerical example considered here, we have found accurate Gaussian beam-tracing results when $\gamma(\boldsymbol{r}, L_x)$ indicates a maximum rate of change in the index of refraction of less than approximately 4% over the beamwidth. It should be noted, however, that this requirement is likely to depend as well on the electrical distance over which the beams are traced. For the example considered here, the beams traveled a distance of over $20\,000\lambda$, presenting a particularly challenging case.

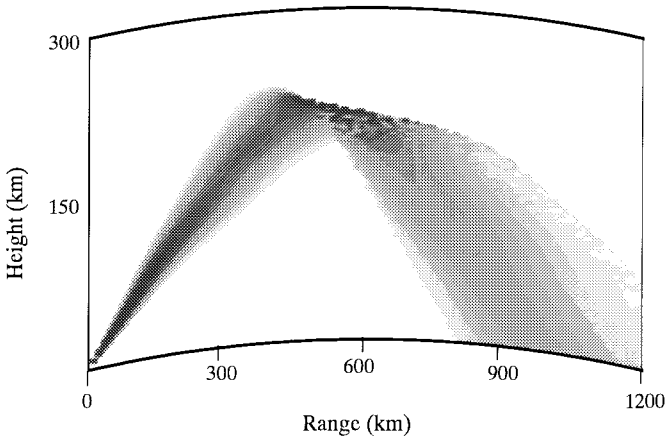

Fig. 10. Results of the full PE solution for the profile in Fig. 2 and initial fields in (21).

Finally, note from Fig. 6 that a minimum final beamwidth is achieved as a function of L_x, dictated by the wavelength λ and the dominant angles of propagation θ_n. Therefore, there is a maximum degree of inhomogeneity that can be tolerated after which λ and θ_n dictate that *no* L_x will provide a beam with sufficient tightness. This reiterates the fact that the beam algorithm is valid for forward-wave propagation along the ray trajectory, thereby assuming smooth variation in the inhomogeneity profile relative to wavelength. However, the OTHR is a particularly challenging example, characterized by severe inhomogeneities and very long-range propagation and the results in Fig. 9 are in close agreement with the full PE solution (for the appropriate L_x).

B. Near-Grazing High-Frequency Radar

As a final example, we consider near-grazing propagation at high frequencies, as addressed in [13]. In particular, we consider an initial field distribution for the wide-angle PE [as in (21)] with $z_o = 50$ m, $\theta_o = 1°$, k is the free-space wavelength for $\lambda = 0.1$ m (frequency of 3 GHz), and $\sigma = 50\lambda$. The ground is treated as in the OTHR example, and the PE is used to compute the fields to a range of 250 km and a height of 100 m with the fields stored at the height $h = 75$ m. These fields are then projected onto the Gabor basis after interpolating the slowly varying range dependence of the PE-computed fields (as for the OTHR problem).

The near-grazing example poses a particularly challenging case for the Gaussian beams, because from (13), the prominent angles of propagation dictate a very large L_x such that a given beamwidth can be achieved. However, for this example, we have the advantage that the inhomogeneity profile is not as severe as in the OTHR problem and, therefore, the beamwidth need not be as tight to satisfy the underlying beam-tracing assumptions. In particular, we utilize one of the inhomogeneity profiles considered in [13], described in terms of the modified refractive index $m(r, z) = n(r, z) + z/a$, introduced by the earth-flattening relationships in (3). Moreover, since z/a is generally a very small quantity, in [13], the parameter $M \equiv 10^6(m - 1)$ is introduced and here we consider $M = 2$ at $z = 0, M = 0$ at $z = 100$ m and $M = 118$ at $z = 1100$ m, with a linear distribution in between ([13, Table II]).

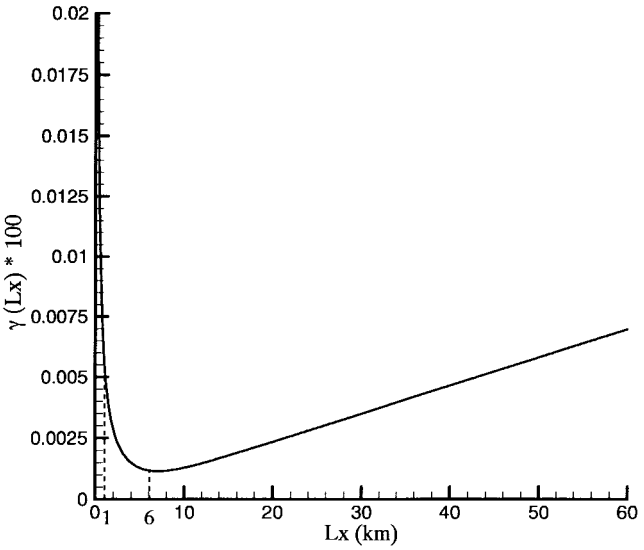

Fig. 11. Variation of the beamwidth as a function of L_x for a beam launched at the angle $i = 1°$, through the inhomogeneous medium described in Section III-B. The beamwidth is measured at a height of $z = 5$ km.

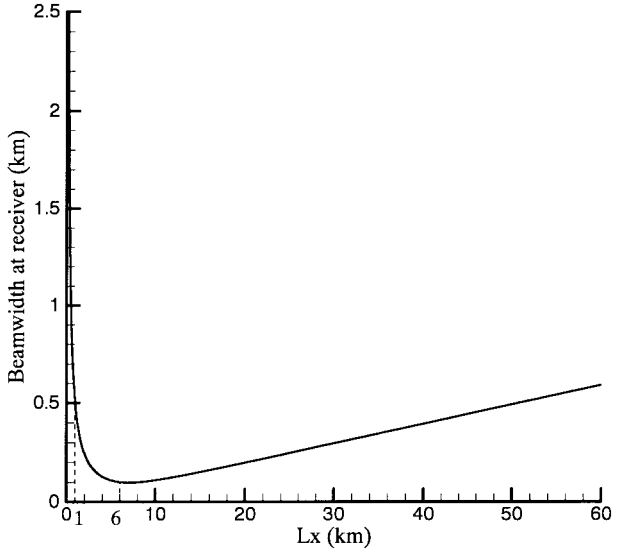

Fig. 12. Change in the index of refraction across a beamwidth, as measured at the height $z = 5$ km for the beam considered in Fig. 11. The change in index of refraction is defined by $\gamma(\boldsymbol{r}, L_x)$ in (20).

In Fig. 11, we plot the beamwidth $B(L_x)$ as measured at the height $z = 5$ km, considering a beam launched at the principal angle $\theta = 1°$. As in the OTHR example (Fig. 6), the beamwidth is quite large for narrow L_x, there is a value of L_x for which B is minimum ($L_x = 6$ km), followed by a subsequent slow increase in $B(L_x)$ for $L_x > 6$ km. The Gabor-generated beams are matched to the beam-tracing algorithm at $z_R = 10\lambda$ at which, as discussed above, the asymptotic results in (11) were found to be quite accurate. For the paraxial approximation [17]–[19] to be valid at $z_R = 10\lambda$, we require an $L_x = 60$ m. Unfortunately, while this value of L_x is sufficient for free-space applications, for the inhomogeneity considered here the subsequent beamwidth $B(L_x)$ is too large for the underlying assumptions in the beam-tracing algorithm (as was found for the OTHR example). To quantify this, in Fig. 12 we plot the parameter $\gamma(\boldsymbol{r}, L_x)$ from (20) as a function of L_x, as measured for a fixed $\boldsymbol{r}$ at $z = 5$ km [as in Fig. 11]. We see that the weak inhomogeneity of this problem (relative to the OTHR example) results in much less material variation over a beamwidth. The minimum variation occurs at the null in Fig. 11, $L_x = 6$ km. For $L_x = 60$ m dictated by the paraxial approximation, the beamwidth is 8.3 km at the observation height $z = 5$ km, thereby encompassing all the inhomogeneity seen in the problem (the beam-tracing results were, therefore, meaningless for this value of L_x).

Finally, in Fig. 13 we plot a comparison of results computed via the full PE solution (over the entire computational domain, as depicted in Fig. 14) with data computed using the hybrid beam-tracing scheme. Results are plotted for $L_x = 1$ and 6 km, as measured at $z = 5$ km [see Fig. 11]. We see that for this example and these parameters, the agreement between the PE and hybrid algorithm is excellent. While in the OTHR example it was found that some of the underlying assumptions in the PE approximation were tenuous (for some observation points) for this example the error in the approximation to $Q(x, z)$ [see (4)] is less than 0.04% over the entire computational domain.

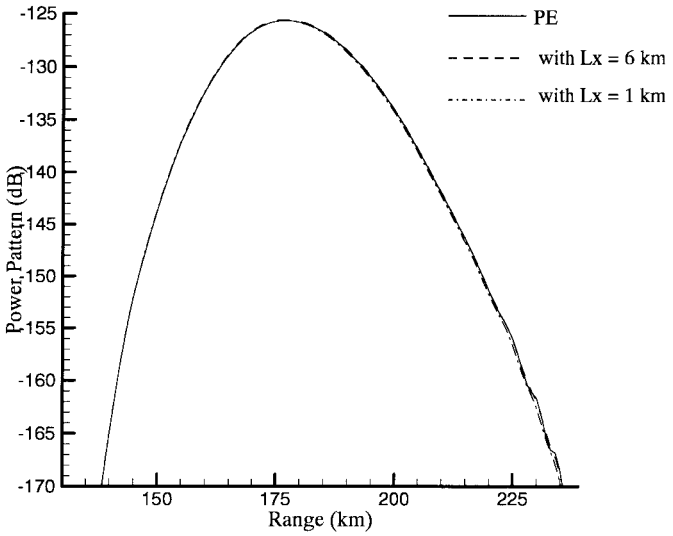

Fig. 13. Power loss at a height of 5 km for near-grazing propagation at 3 GHz for the inhomogeneity profile considered in Figs. 11 and 12. Results are compared between a full PE algorithm (for the entire computational domain) and the hybrid PE (Gabor expansion–beam-tracing) algorithm for two values of Gabor width L_x.

C. Numerical Issues and Comparisons with Other Algorithms

As indicated above, if L_x used in the Gabor expansion is sufficiently large to assure a tight Gaussian beam, relative to the material inhomogeneity, the hybrid (Gabor-transform)–(beam-tracing) algorithm results in highly accurate results, as compared with an independent (PE) solution. Nevertheless, we address here several numerical issues which highlight the advantages and disadvantages of this algorithm. A principal shortcoming is the need to compute the coefficients of the Gabor expansion functions, often when L_x is quite large relative to wavelength. In particular, in the second example (Section III-B) we considered $L_x = 1$ and 6 km, $33\,333\lambda$, and $200\,000\lambda$, respectively. We utilize the bi-orthogonality

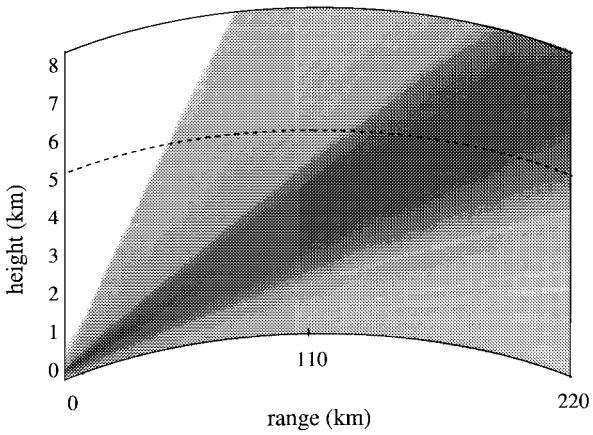

Fig. 14. Results of the full PE computation for the problem in Fig. 13.

relationship

$$a_{mn} = \int_{-\infty}^{\infty} f(x)\beta^*(x - mL_x)\exp(jnk_x x)\,dx$$

$$\beta(x) = (\sqrt{2}L_x)^{-1/2}\left(\frac{K_o}{\pi}\right)^{-3/2}\exp[-\pi(x/L_x)^2] \cdot \sum_{l\geq l_o}^{\infty}(-1)^l\exp[-\pi(l+1/2)^2] \tag{22}$$

where $l_o = (x/L_x) - 1/2$ and $K_o = 1.854\,074\,68$. The integral in (22) was computed via Gauss–Legendre integration and, for the example in Section III-B, this required several hours of CPU on a Pentium PC. The subsequent beam tracing is, by contrast, quite efficient. Therefore, for this example, characterized by a small wavelength and near-grazing propagation, the algorithm yields highly accurate results at a relatively significant computational expense.

The horizontal PE algorithm in [13] has the advantage that vertical propagation is solved using the reduced form of the fields and, therefore, the highly oscillatory term in the x direction is eliminated (as is conventional in PE solutions). Therefore, one does not suffer the problems discussed above with regard to subwavelength sampling in the x direction. However, while the scheme in [13] is more efficient computationally in this respect, it is applicable only to standard inhomogeneities.

Considering the OTHR example of Section III-A, the ionospheric profile does not fit readily into a standard form. Moreover, note from Fig. 10 that the fields are reflected back toward the earth, posing a particular challenge for a forward-marching horizontal-PE scheme. For the problem in Section III-A, we required a Gabor width $L_x/lambda = 400$ and, therefore, the computations in (22) were relatively efficient (several minutes on a personal computer) and, therefore, the Gabor-beam algorithm is quite efficient.

Finally, with regard to (22) and (9), in general one must evaluate amn for each propagating beam. For the large L_x considered in Sections III-A and B, this implies a very large number of modes. However, we are generally only interested in the fields radiated in a particular direction or region. Thus, knowing the launch angles of the beams, we have advance knowledge of which beams are necessary for the representation of the fields in a given region. Moreover, one can neglect beams with very small amplitudes a_{mn} contributing minimally to the total fields. For example, in the example in Section III-B, most of the energy travels at the angle $\theta = 1°$ and, therefore, only beams traveling near this angle are of principal concern. Taking into account these considerations (for the example in Fig. 9), we used 100 beams for $L_x = 12$ km, while for the results in Fig. 13, we used 300 and 25 beams, respectively, for $L_x = 1$ km and $L_x = 6$ km.

In summary, several algorithms have been developed over the years for the propagation of fields (PE computed or otherwise) away from an aperture into a inhomogeneous medium. It is felt that no one algorithm can be viewed as optimal, each having their respective domains of advantage. For particular classes of inhomogeneity, Green's function [14] or ray-based [15] schemes are quite effective. Moreover, for standard inhomogeneities the horizontal PE scheme is very accurate and efficient [13]. The hybrid Gabor-beam algorithm presented here appears to be a useful tool for problem types for which these other algorithms have problems: in regions for which the material is nonstandard or for which there is reflection back toward the earth (cf., [13]), for which there are caustics or shadow boundaries (cf. [15]) and for which a Green s function is difficult to obtain (cf., [14]). These criteria are naturally met for a problem of the type considered in Section III-A (OTHR). On the other hand, while the example in Section III-B demonstrated the accuracy of the Gabor-beam scheme, a problem of this type is more efficiently handled with the algorithm in [13] (from where this example was taken).

IV. Conclusions

A hybrid PE (Gaussian beam) algorithm has been developed for the long-range propagation of fields through complicated inhomogeneous environments. The PE computed fields are stored along an aperture and then projected onto a complete Gabor basis, each Gabor basis function giving rise to a tilted Gaussian beam. These Gaussian beams are then used as starter fields for a Gaussian beam algorithm, which is applicable for propagation through general inhomogeneous environments. The Gaussian beam algorithm applies the PE approximation for forward propagation along ray trajectories each of which is initiated at the center of the tilted Gaussian beam starter fields. The beam-tracing algorithm, therefore, represents an improvement on conventional ray tracing in that it uses conventional ray trajectories yet, by utilizing fields that extend beyond the trajectory, it circumvents artifacts at caustics and shadow boundaries. Further, the Gabor basis functions provide a rigorous and self-consistent coupling of the PE algorithm (or any numerical algorithm) with beam tracing; such a coupling is difficult with conventional ray tracing.

Example results were presented for a realistic over-the-horizon radar (OTHR) scenario as well as for a near-grazing high-frequency radar example. These examples allowed us to address several numerical issues associated with this algorithm. In particular, previous work on Gabor-launched beams with application to free-space problems has identified two

mathematical constraints on the Gabor expansion functions. In particular, for a given distance away from the Gabor function (i.e., from the aperture), the Gabor width L_x must be chosen sufficiently large to satisfy the paraxial approximation and the underlying assumptions in the asymptotic derivation of (11). We have demonstrated that the presence of inhomogeneous media introduces a new constraint on L_x, essential for subsequent beam tracing. In particular, L_x must be sufficiently large such that the beam is tight enough relative to the material inhomogeneity to satisfy the underlying beam-tracing assumption: that the beam fields are dictated primarily by the material properties along the beam axis. For the examples considered here, this latter restriction was found more severe (required larger L_x) than either of the former two.

With regard to the projection of the aperture fields onto a Gabor basis, the Gabor basis functions constitute elements with constant support in the spatial–spectral phase space [28] (more commonly viewed in time-frequency). Over the last several years, however, substantial research has been performed on wavelets, which are characterized by multiresolution in the phase space [29], [30]. Further, wavelets have proven to provide substantial compression for function (image) representation. Thus, a potentially fruitful avenue of future research involves investigation of projecting the aperture fields onto a wavelets basis, which may reduce the number of beams vis-à-vis the Gabor basis. However, in this context, the choice of wavelet is critical, for the wavelets must provide good propagators. As discussed in Section II-B, the Gabor basis functions naturally give rise to tilted Gaussian beams. Similar properties must hold for the wavelet basis selected if they are to be useful for wave- propagation applications.

REFERENCES

[1] M. Skolnik, *Radar Handbook*, 2nd ed. New York: McGraw-Hill, 1990.

[2] M. F. Levy, "Diffraction studies in urban environments with wide angle parabolic equation method," *Electron. Lett.*, vol. 28, no. 16, pp. 1491–1492, July 1992.

[3] G. L. James, *Geometrical Theory of Diffraction for Electromagnetic Waves*, 3rd ed. London, U.K.: Peregrinus, 1986.

[4] K. S. Kunz and R. J. Luebbers, *The Finite Difference Time Domain Method for Electromagnetics*. Boca Raton, FL: CRC, 1993.

[5] R. F. Harrington, *Field Computation by Moment Methods*. Malabar, FL: Kreiger, 1985.

[6] P. Silvester, *Finite Elements for Electrical Engineers*. New York: Cambridge Univ. Press, 1990.

[7] M. A. Leontovich and V. A. Fock, "Solution of the problem of propagation of electromagnetic waves along the earth's surface by the method of parabolic equations," *J. Phys. USSR*, vol. 10, pp. 13–24, 1946.

[8] R. H. Hardin and F. D. Tappert, "Application of the split-step Fourier method to the numerical solution of nonlinear and variable coefficient wave equations," *SIAM Rev.*, vol. 15, p. 423, 1973.

[9] M. D. Feit and J. A. Fleck, Jr., "Light propagation in graded-index fibers," *Appl. Opt.*, vol. 17, pp. 3990–3998, Dec. 1978.

[10] D. J. Thomson and N. R. Chapman, "A wide-angle split-step algorithm for the parabolic equation," *J. Acoust. Soc. Amer.*, vol. 74, pp. 1848–1854, Dec. 1983.

[11] D. D. Dockery, "Modeling electromagnetic wave propagation in the troposphere using the parabolic equation," *IEEE Trans. Antennas Propagat.*, vol. 36, pp. 1464–1470, Oct. 1988.

[12] F. J. Ryan, "Analysis of electromagnetic propagation over variable terrain using the parabolic wave equation," Naval Ocean Syst. Ctr., San Diego, CA, Tech. Rep. 1453, Oct. 1991.

[13] M. F. Levy, "Horizontal parabolic equation solution of radiowave propagation problems on large domains," *IEEE Trans. Antennas Propagat.*, vol. 43, pp. 137–144, Feb. 1995.

[14] S. H. Marcus, "A hybrid (finite difference-surface Green's function) method for computing transmission losses in an inhomogeneous atmosphere over irregular terrain," *IEEE Trans. Antennas Propagat.*, vol. 40, pp. 1451–1458, Dec. 1992.

[15] H. V. Hitney, "Hybrid ray optics and parabolic equation methods for radar propagation modeling," in *Inst. Elect. Eng. Conf. Proc. Radar*, Brighton, U.K., Oct. 1992, pp. 58–61.

[16] J. M. Headrick and M. I. Skolnik, "Over-the-horizon radar in the HF band," *Proc. IEEE*, vol. 62, pp. 664–673, June 1974.

[17] J. J. Maciel and L. B. Felsen, "Systematic study of fields due to extended apertures by Gaussian beam discretization," *IEEE Trans. Antennas Propagat.*, vol. 37, pp. 884–892, July 1989.

[18] ———, "Gaussian beam analysis of propagation from an extended plane aperture distribution through dielectric layers—I: Plane layer, —II: Circular cylindrical layer," *IEEE Trans. Antennas Propagat.*, vol. 38, pp. 1608–1624, Oct. 1990.

[19] P. D. Einziger, S. Raz, and M. Shapira, "Gabor representation and aperture theory," *J. Opt. Soc. Amer.*, vol. 3, pt. A, pp. 508–522, Apr. 1986.

[20] V. Červený, M. M. Popov, and I. Pšenčik, "Computation of wave fields in inhomogeneous media-Gaussian beam approach," *Geophys. J. R. Astron. Soc.*, vol. 70, pp. 109–128, 1982.

[21] M. B. Porter and H. P. Bucker, "Gaussian beam tracing for computing ocean acoustic fields," *J. Acoust. Soc. Amer.*, vol. 82, pp. 1349–1359, Oct. 1987.

[22] M. H. L. Pryce, "The diffraction of radio waves by the curvature of the earth," *Adv. Phys.*, vol. 2, pp. 67–95, 1953.

[23] C. L. Pekeris, "Accuracy of the earth-flattening approximation in the theory of microwave propagation," *Phys. Rev.*, vol. 70, pp. 518–522, 1946.

[24] M. H. Reilly and E. L. Strobel, "Efficient ray tracing through a realistic ionosphere," *Radio Sci.*, vol. 23, pp. 247–256, Mar. 1988.

[25] L. B. Felsen and N. Marcuvitz, *Radiation and Scattering of Waves*. Englewood Cliffs, NJ: Prentice-Hall, 1973, ch. 4; New York: IEEE Press, 1995.

[26] F. B. Jensen, W. A. Kuperman, M. B. Porter, and H. Schmidt, *Computational Ocean Acoustics*. New York: AIP, 1994, ch. 3.

[27] J. M. Kelso, *Radio Ray Propagation in the Ionosphere.* New York: McGraw-Hill, 1964.

[28] L. Cohen, "Time-frequency distributions—A review," *Proc. IEEE*, vol. 77, pp. 941–981, July 1989.

[29] S. G. Mallat, "A theory for multiresolution signal decomposition: The wavelet representation," *IEEE Trans. Pattern Anal. Mach. Intell.*, vol. 11, pp. 674–693, July 1989.

[30] I. Daubechies, "The wavelet transform, time-frequency localization and signal analysis," *IEEE Trans. Inform. Theory*, vol. 36, pp. 961–1005, Sept. 1990.

Bimba Rao was born in Mysore, India, on November 27, 1973. She received the B.E. degree in electronics and telecommunication engineering from College of Engineering, Pune, India, in 1995, and the M.S. degree in electrical engineering from Duke University, Durham, NC, in 1997. She is currently working toward the Ph.D. degree at Duke University.

Her research interests include computational electromagnetics as applied to inverse imaging problems.

Lawrence Carin (SM'96) was born on March 25, 1963, in Washington, DC. He received the B.S., M.S., and Ph.D. degrees in electrical engineering at the University of Maryland, College Park, in 1985, 1986, and 1989, respectively.

In 1989, he joined the Electrical Engineering Department at Polytechnic University, Brooklyn, NY, as an Assistant Professor, and became an Associate Professor there in 1994. In September 1995 he joined the Electrical Engineering Department at Duke University, where he is currently an Associate Professor. His current research interests include quasi-planar transmission lines, short-pulse scattering and propagation, and signal processing.

Dr. Carin is a member of the Tau Beta Pi and Eta Kappa Nu honor societies.